Simulating ozone dry deposition at a boreal forest with a multi-layer canopy deposition model

Putian Zhou[1], Laurens Ganzeveld[2], Üllar Rannik[1], Luxi Zhou[1, *], Rosa Gierens[1, **], Ditte Taipale[3,4], Ivan Mammarella[1], and Michael Boy[1]

[1]University of Helsinki, Department of Physics, P.O. Box 64, FI-00014, University of Helsinki, Finland
[2]Meteorology and Air Quality (MAQ), Department of Environmental Sciences, Wageningen University and Research Centre, Wageningen, Netherlands
[3]University of Helsinki, Department of Forest Sciences, P.O. Box 27, FI-00014, University of Helsinki, Finland
[4]Estonian University of Life Sciences, Department of Plant Physiology, Kreutzwaldi 1, EE-51014, Estonia
[*]now at U.S. Environmental Protection Agency, Research Triangle Park, NC, USA
[**]now at Institute for Geophysics and Meteorology, University of Cologne, Germany
Correspondence to: Zhou Putian (putian.zhou@helsinki.fi)

Abstract. A multi-layer ozone (O_3) dry deposition model has been implemented into SOSAA (a model to Simulate the concentrations of Organic vapours, Sulphuric Acid and Aerosols) to improve the representation of O_3 concentration and flux within and above the forest canopy in the planetary boundary layer. We aim to predict the O_3 uptake by a boreal forest canopy under varying environmental conditions and analyse the influence of different factors on total O_3 uptake by the canopy as well as

5   the vertical distribution of deposition sinks inside the canopy. The newly implemented dry deposition model was validated by an extensive comparison of simulated and observed O_3 turbulent fluxes and concentration profiles within and above the boreal forest canopy at SMEAR II (the Station to Measure Ecosystem-Atmosphere Relation II) in Hyytiälä, Finland, in August, 2010.

In this model, the fraction of wet surface on vegetation leaves was parametrised according to the ambient relative humidity (RH). Model results showed that when RH was larger than 70% the O_3 uptake onto wet skin contributed $\sim 51\%$ to the total

10   deposition during nighttime and $\sim 19\%$ during daytime. And the overall contribution of soil uptake was estimated about 36%. The contribution of sub-canopy deposition below 4.2 m was modelled to be $\sim 38\%$ of the total O_3 deposition during daytime which was similar to the contribution reported in previous studies. The chemical contribution to O_3 removal was evaluated directly in the model simulations. According to the simulated averaged diurnal cycle the net chemical production of O_3 compensated up to $\sim 4\%$ of dry deposition loss from about 06:00 to 15:00. During nighttime, the net chemical loss of O_3

15   further enhanced removal by dry deposition by a maximum $\sim 9\%$. Thus the results indicated that an overall relatively small contribution by airborne chemical processes to O_3 removal at this site.

1 Introduction

Tropospheric ozone (O_3) is an important oxidant of many reactive species such as biogenic volatile organic compounds (BVOCs) emitted from the forest canopy (Bäck et al., 2012; Smolander et al., 2014). It also plays a significant role in the

20   regulation of the atmospheric oxidation capacity first of all by being one of the primary sources of the hydroxyl radical (OH)

which is the most critical oxidant in the air (Mogensen et al., 2015). O_3 also initiates the formation of Criegee intermediate (CI) radicals which are crucial in tropospheric oxidation (Boy et al., 2013). As an air pollutant, O_3 can cause damage to human health (Kampa and Castanas, 2008) and affect ecosystem functioning via its various toxic impacts (Felzer et al., 2007). O_3 can also alter the global radiative forcing as an important greenhouse gas (Stocker et al., 2013, chap. 2). Hence it is impor-

5 tant to understand the O_3 budget including its sources and sinks at local or site scale in order to understand the global scale implications.

O_3 is produced via photochemical reactions in the presence of precursor gases, e.g., volatile organic compounds (VOCs), CO (carbon oxide), OH and NO_x (nitric oxide and nitrogen dioxide) or transported downward from stratosphere, and is removed mainly near the Earth's surface. For vegetated surfaces a large part of the removal processes are via stomatal uptake on leaf

10 surface and non-stomatal uptake on plant canopies and soil surface (Wesely, 1989; Ganzeveld and Lelieveld, 1995; Altimir et al., 2006; Rannik et al., 2012; Launiainen et al., 2013), as well as depleted by chemical reactions (Kurpius and Goldstein, 2003; Wolfe et al., 2011). In this study we focus on the O_3 removal and production processes within and immediately above the canopy, more particularly on the O_3 uptake by boreal forest which covers 33% of global forest land (Ruckstuhl et al., 2008).

For vegetation, the uptake of O_3 depends on the turbulence intensity above and within the canopy, the diffusive transfer in

15 the quasi-laminar boundary layer over the leaf surface, the biological properties of the plants, surface wetness condition, and soil type (Ganzeveld and Lelieveld, 1995). Among them the effect of canopy wetness on O_3 deposition has attracted a lot of attention in previous studies (e.g., Massman, 2004; Altimir et al., 2006). For different vegetation types and under different environmental conditions the surface wetness can enhance or reduce O_3 deposition (Massman, 2004). For a boreal forest, a number of studies have revealed an enhancement of the O_3 uptake under dew or high humidity conditions. For example,

20 Lamaud et al. (2002) reported that dew on canopy surface significantly increased the O_3 uptake at night and in the morning over a pine stand. Altimir et al. (2006) also found that the condensed moisture on the surfaces enhanced the non-stomatal O_3 uptake in a Scots pine forest when ambient relative humidity (RH) was over 60 - 70%. Similarly to Altimir et al. (2006), Rannik et al. (2012) revealed a strong sensitivity of the nighttime O_3 uptake to RH. The enhancement of O_3 uptake on wet leaf surface was also explained by previous studies which showed that both the micro structure of the leaf surface and the hydrophilic

25 compounds existing on the leaf surface are able to facilitate the formation of the water films or clusters, although the foliage surface itself is hydrophobic (Altimir et al., 2006). As a result, the different dissolved compounds like organics in the solution formed on leaf surface could react with O_3 and thus enhance the O_3 uptake (Altimir et al., 2006).

In addition, the boreal forest emits a large portion of BVOCs (Rinne et al., 2009) which are considered to play a significant role in non-stomatal removal of O_3 by oxidation in several studies (Kurpius and Goldstein, 2003; Goldstein et al., 2004; Wolfe

30 et al., 2011). For example, Fares et al. (2010) found the correlation between the oxidation products of monoterpenes and O_3 non-stomatal flux at a ponderosa pine stand in California, US, indicating the gas-phase reactions of O_3 with BVOCs were mostly responsible for O_3 non-stomatal loss. In a model study, Wolfe et al. (2011) suggested that the non-stomatal O_3 uptake at the same Californian site could be explained by considering the role of O_3 destruction with the presence of very reactive BVOCs. Consequently, further analysis of the role of non-stomatal removal of O_3 also strongly depends on the improvement

35 of BVOCs measurement. However, the influence of this gas-phase chemical removal process may vary among different sites.

A study by Rannik et al. (2012), who conducted a detailed analysis of a long-term O_3 deposition flux measurement at a boreal forest station in Hyytiälä, Finland, indicated that, at the currently known strength of BVOC emissions, the air chemistry of BVOCs was not likely an important O_3 sink term at this site.

In recent two decades, several numerical models have been developed to study and simulate O_3 dry deposition processes under different climatic and environmental conditions. Many of them have implemented the big-leaf framework following the Wesely (1989) approach which can be coupled to regional or global models to estimate the O_3 deposition flux in large scales (e.g., Hardacre et al., 2015). However, the "big-leaf" approach does not consider explicitly the role of in-canopy interactions between biogenic emissions, chemistry, turbulence and deposition. Therefore, more detailed multi-layer models including the role of these in-canopy interactions have been developed and applied to analyse in-canopy deposition-related mechanisms (e.g., Ganzeveld et al., 2002b; Rannik et al., 2012; Launiainen et al., 2013). These multi-layer canopy exchange models have also been coupled to large scale models, e.g., a global chemistry-climate model system (Ganzeveld et al., 2002a), or have been implemented in column models with detailed vertically separated layers (e.g., Wolfe and Thornton, 2011).

In this study a multi-layer O_3 dry deposition model was implemented into the 1-dimension (1D) chemical transport model SOSAA (a model to Simulate the concentrations of Organic vapours, Sulphuric Acid and Aerosols). This deposition model was based on the dry deposition representation originally described in Ganzeveld and Lelieveld (1995) and Ganzeveld et al. (1998) and implemented in the Multi-Layer Canopy CHemistry Exchange Model (MLC-CHEM, Ganzeveld et al. (2002b)). This canopy exchange system in MLC-CHEM was already applied in a single column model on the analysis of site-scale exchange processes (Ganzeveld et al., 2002b; Seok et al., 2013), as well as in a global chemistry-climate model system on the analysis of atmosphere-biosphere exchange processes (Ganzeveld et al., 2002a, 2010).

Furthermore, the long-term continuous measurements and extensive campaigns at SMEAR II have provided a vast amount of data with complementary information on micrometeorology as well as O_3 fluxes and concentrations, which are highly appropriate for validating the new model and investigating more detailed processes. We selected a featured month August 2010 for such an extensive evaluation of the model because this month was characterised by exceptional hot and dry conditions in the first two weeks, which possibly represented a future climate at this site (Williams et al., 2011), then followed by two cooler weeks. This study is a starting point of investigating gas dry deposition processes by using SOSAA. We aim to evaluate not only quantitatively O_3 fluxes and concentration profiles but also the role of individual deposition processes at this site. This is a prerequisite for a further analysis of BVOCs deposition and chemistry in the follow-up research.

In the following section, a detailed description of the measurement and model will be shown. The comparisons between simulated and observed meteorological quantities, O_3 fluxes above the canopy and O_3 concentration profiles are described in section 3, as well as the discussion about O_3 flux profiles and the impact of air chemistry. Finally, a summary is given in section 4.

2 Methods

2.1 Site

All the measurement data used in this study were from SMEAR II (the Station to Measure Ecosystem-Atmosphere Relation II) located in Hyytiälä, Finland (61°51'N, 24°17'E, 181 m above the sea level) (Hari and Kulmala, 2005). The boreal coniferous

5   forest is relatively homogeneous around the station in all the directions within 200 m, 75% covered by Scots pine (*Pinus sylvestris*) and the rest covered by Norway Spruces (*Picea abies*) and deciduous trees (Bäck et al., 2012). The understory vegetation mainly consists of lingonberry (*Vaccinium vitis-idaea*) and blueberry (*Vaccinium myrtillus*) with a mean height of 0.2 - 0.3 m. The forest floor is covered by dense mosses, mostly *Dicranum polysetum*, *Hylocomium splendens* and *Pleurozium schreberi*. Underneath is a 5 cm layer of humus in soil (Kolari et al., 2006; Kulmala et al., 2008). In 2010, the tree height

10   reaches around 18 m. The all-sided leaf area index (LAI) is about 7.5 m^2 m^{-2}, including $\sim$ 6.0 m^2 m^{-2} overstory vegetation, $\sim$ 0.5 m^2 m^{-2} understory vegetation and $\sim$ 1 m^2 m^{-2} moss layer (Launiainen et al., 2013). The vertical profiles of LAI and leaf area density (LAD) are shown in Fig. 1.

2.2 Measurements

The measurement data at SMEAR II are currently publicly available in the data server maintained by AVAA open data pub-

15   lishing platform (http://avaa.tdata.fi/web/smart/smear), which was originally introduced in Junninen et al. (2009). A part of observed quantities used in this study are available at 4.2 m, 8.4 m, 16.8 m, 33.6 m, 50.4 m and 67.2 m above the ground level, including air temperature (measured by Pt100 sensor), air water content (Li-Cor LI-840 infrared light absorption analyser) and O_3 concentration (TEI 49C ultraviolet light absorption analyser). Other observed quantities include the photosynthetically active radiation (PAR, 400–700 nm) (Li-Cor Li-190SZ quantum sensor) measured at 18 m, PAR (array of 4 Li-Cor Li-190SZ

20   sensors) measured at 0.6 m, net radiation (Reeman MB-1 net radiometer) at 67 m, O_3 flux (Gill Solent HS 1199 sonic anemometer & Unisearch Associates LOZ-3 gas analyzer) at 23 m, friction velocity (Gill Solent 1012R anemometer/themometer) at 23 m, sensible and latent heat fluxes (H and LE) (Gill Solent 1012R and Li-Cor LI-6262 gas analyzer) at 23 m, and soil heat flux (Hukseflux HFP01 heat flux sensors).

   In this study the measured O_3 fluxes were calculated over 30 min averaging period using the EddyUH software (Mammarella

25   et al., 2016) and according to standard methodology (for more details see Rannik et al., 2012). Other variables were also half-hour averaged to fit the model time step for both input and output. The air temperature (T), RH and O_3 concentration were linearly interpolated using the observations collected at a height of 16.8 m and 33.6 m to arrive at the estimated parameter values at 23 m to allow a direct comparison of the model results with the measurements or being used as input for the model. The missing observed data points of T, RH and O_3 were gap-filled with the method described in Gierens et al. (2014).

30   The measured O_3 fluxes were filtered based on the fact that previous studies showed that the measured fluxes had large errors under very low turbulence (Rannik et al., 2006). The threshold of such low turbulence condition was usually set according to the measured friction velocity on top of the canopy in the range of 0.1 m s^{-1} to 0.25 m s^{-1} (Altimir et al., 2006; Rannik et al., 2012; Launiainen et al., 2013). Here the observed O_3 fluxes were excluded when $u_* \leqslant 0.2$ m s^{-1} which was proposed

by Rannik et al. (2012). Secondly, the O_3 flux measurements were filtered out when precipitation occurred within preceding 1 hour. Previous studies used a more strict criteria for such a filter that the preceding 12 hours should keep dry to ensure dry canopy conditions (Altimir et al., 2006; Launiainen et al., 2013). However, in this study the fraction of wet canopy skin was taken into account and consequently we applied the filtering criteria of 1 hour. Overall, 60% of O_3 flux data were available compared to 87% prior to filtering.

Here we should notice that the fluxes determined by the eddy-covariance (EC) technique were affected by the stochastic nature of turbulence, revealing as the random uncertainty of 30 min average fluxes. For the EC measurement the random uncertainty was typically in the order of ten to a few tens of percent. For the O_3 turbulent flux measurement at the same site Keronen et al. (2003) presented the random error statistics, defined as one standard deviation of the random uncertainty of turbulent flux, ranging from about 10 to 40%.

2.3 Classification of time period

Previous studies showed that in pine forest RH could enhance non-stomatal O_3 uptake (Lamaud et al., 2002; Altimir et al., 2006; Rannik et al., 2012), especially during nighttime (Rannik et al., 2012). Hence in order to further analyse the impact of RH, the data were separated into different groups according to daytime (D) and nighttime (N) as well as RH measured inside the canopy, representing the daytime with high humidity condition (DH), daytime with low humidity condition (DL), nighttime with high humidity condition (NH) and nighttime with low humidity condition (NL). The data points were considered as daytime when the sun elevation angle was larger than $10°$ and as nighttime when the sun elevation angle was smaller than $0°$. The RH threshold value was set to 70% referring to previous studies (Altimir et al., 2006; Rannik et al., 2012), so a period is in high humidity condition when all the measured RH values inside the canopy are higher than 70%, similarly a period is in low humidity condition when all the measured RH values inside the canopy are lower than 70%. For O_3 flux, "ALL" was used to represent the time period with all available data after filtering described in section 2.2.

2.4 Model description

2.4.1 SOSAA

SOSAA is a 1D chemical transport model which couples different modules to simulate the emissions of BVOCs, chemical reactions of organic and inorganic compounds in the air, transportation of trace gases and aerosol particles, as well as the aerosol processes within and above the canopy in the planetary boundary layer. It was first introduced as SOSA by Boy et al. (2011) based on the 1D version of SCADIS (SCAlar DIStribution, Sogachev et al., 2002). After that an aerosol module based on UHMA (University of Helsinki Multicomponent Aerosol model, Korhonen et al., 2004) was implemented by Zhou et al. (2014) resulting in its name being changed to SOSAA. The current version of SOSAA includes five modules. The meteorology module is based on SCADIS. Emissions of BVOCs from the canopy are calculated by the Model of Emissions of Gases and Aerosols from Nature (MEGAN, Guenther et al., 2006). The Master Chemical Mechanism version 3.2 (MCMv3.2) (http://mcm.leeds.ac.uk/MCM) has been implemented to provide chemistry information. The nucleation, condensation, coagulation

and deposition of aerosol particles are described by UHMA. In this study a gaseous compound dry deposition module has been implemented into SOSAA. SOSAA has already been applied and verified in several studies (e.g., Kurtén et al., 2011; Mogensen et al., 2011; Boy et al., 2013; Mogensen et al., 2015; Bäck et al., 2012; Smolander et al., 2014; Zhou et al., 2015).

In SOSAA, the horizontal wind velocity (u and v), T, specific humidity (q_v), turbulent kinetic energy (TKE) and the specific dissipation of TKE (ω) are computed every time step (10 s) by prognostic equations. In order to represent the local to synoptic scale effects, u, v, T and q_v near and within the canopy are nudged to local measurement data at SMEAR II station with a nudging factor of 0.01. A TKE-ω parametrisation scheme is used to calculate the turbulent diffusion coefficient (K_t) (Sogachev, 2009),

$$K_t = C_\mu \frac{\text{TKE}}{\omega} \tag{1}$$

$$\omega = \frac{\varepsilon}{\text{TKE}} \tag{2}$$

where ε is the dissipation rate of TKE and C_μ (0.0436) is a closure constant. Hence the turbulent flux of a quantity X ($F_{t,X}$) can be computed as

$$F_{t,X} = -K_t \frac{\partial X}{\partial z} \tag{3}$$

where upward fluxes are positive and vice versa. Specifically, the sensible heat flux (H) and latent heat flux (LE) at each model layer are computed as

$$\text{H} = -C_{p,air} \rho_{air} K_h \left(\frac{\partial T}{\partial z} + \gamma_d \right) \tag{4}$$

$$\text{LE} = -L_v K_h \frac{\partial q_v}{\partial z} \tag{5}$$

where $C_{p,air}$ (1009.0 J kg^{-1} K^{-1}) is the specific heat capacity at constant pressure. ρ_{air} (1.205 kg m^{-3}) is the air density which is a constant in the model. γ_d (0.0098 K m^{-1}) is the lapse rate of dry air. L_v (2.256×10^6 J kg^{-1}) is the latent heat of vaporisation for water. K_h is the turbulent eddy diffusivity for heat fluxes, which is derived from K_t according to the atmospheric stability.

The upper boundary values of u, v, T and q_v are constrained by the ERA-Interim reanalysis dataset provided by the European Centre for Medium-Range Weather Forecasts (ECMWF, Dee et al., 2011). Above the canopy, the incoming direct and diffuse global radiations measured at SMEAR II station, and the long wave radiation obtained from the ERA-Interim dataset are read in to improve the energy balance closure. Then the reflection, absorption, penetration and emission of three bands of radiation (long-wave, near-infrared and PAR) at each layer inside the canopy are explicitly computed according to the radiation scheme proposed by Sogachev et al. (2002). At the lower boundary, the measured soil heat flux at SMEAR II is used to further improve the representation of surface energy balance. All the input data are interpolated to match the model time for each time step. With the input data, the mass and energy exchange between atmosphere and plant cover (including the soil underneath) and the radiation attenuation inside the canopy are optimal to simulate the micrometeorological drivers of O$_3$ deposition at this site.

In current SOSAA, a modified version of MEGAN has been used to simulate the emissions of BVOCs from the trees. The emissions of some important BVOCs are included, e.g., monoterpenes (α-pinene, β-pinene, Δ^3-carene, limonene, cineol and

other minor monoterpenes (OMT)), sesquiterpenes (farnesene, β-caryophyllene and other minor sesquiterpenes (OSQ)) , 2-methyl-3-buten-2-ol (MBO). The chemistry mechanism is from MCMv3.2 including needed inorganic reactions and the full MCM oxidation paths for methane (CH$_4$), isoprene, MBO, α-pinene, β-pinene, limonene and β-caryophyllene. We have also included the first-order oxidation reactions with OH, O$_3$, NO$_3$ for cineole, Δ^3-carene, OMT, farnesene and OSQ. The related

5   chemical reactions of stabilised Criegee intermediates (sCIs) with updated reaction rates from Boy et al. (2013) are also taken into account in current simulations. For more details about emissions and chemistry we refer to Mogensen et al. (2015).

2.4.2   Multi-layer O$_3$ dry deposition model

A gas dry deposition model has been implemented into SOSAA to investigate the influence of the dry deposition processes on the atmosphere-biosphere gas exchange and in-canopy gas concentrations. In this study we focus on the O$_3$ dry deposition

10   since it is the basis of calculating the uptake of other trace gases, including BVOCs (Wesely, 1989). In this multi-layer dry deposition model the O$_3$ deposition flux is calculated at each layer as

$$F_i = -[O_3]_i \cdot V_{d,i} \qquad (i = 1, \ldots, N) \tag{6}$$

where F is the O$_3$ deposition flux (μg m^{-2} s^{-1}), [O$_3$] is the O$_3$ concentration (μg m^{-3}), V_d is the layer-specific conductance (m s^{-1}). The subscript i represents layer index. Layer 1 is the bottom layer including the soil surface and the understory

15   vegetation where the moss layer is considered as part of the soil surface for simplicity. The overstory layers 2 to N include only vegetation surface, where N is the layer index at the canopy top.

V_d is calculated for bottom layer (layer 1) and overstory layers (layers 2 to N) differently. In addition, the deposition onto dry and wet parts of the leaf surface is considered separately. In overstory layers, only the deposition onto leaves is taken into account, while in the bottom layer the additional pathway of deposition onto the soil surface exists. Thus

20   $$V_{d,i} = \frac{\text{LAI}_i}{r_{veg,i}} + \frac{\delta_{i1}}{r_{ac} + r_{bs} + r_{soil}}. \tag{7}$$

Here LAI$_i$ is the all-sided leaf area index for each layer (m^2 m^{-2}). The Kronecker delta δ_{i1} ($\delta_{i1} = 1$ when $i = 1$; $\delta_{i1} = 0$ when $i \neq 1$) is introduced here to simplify the formula.

r_{veg} is the leaf surface resistance which represents how O$_3$ finally deposits onto different parts of leaf surface (Fig. 1). It can be calculated at each layer for needle leaves as

25   $$r_{veg} = r_b + \frac{1}{1/(r_{stm} + r_{mes}) + (1 - f_{wet})/r_{cut} + f_{wet}/r_{ws}}. \tag{8}$$

While for broad leaves, O$_3$ can deposit on a side without stomata or a side with stomata, hence r_{veg} is computed in a different way as

$$r_{veg} = 2 \left/ \left(\frac{1}{r_{veg1}} + \frac{1}{r_{veg2}} \right) \right. \tag{9}$$

$$r_{veg1} = r_b + \frac{1}{(1 - f_{wet})/r_{cut} + f_{wet}/r_{ws}} \tag{10}$$

30   $$r_{veg2} = r_b + \frac{1}{1/(r_{stm} + r_{mes}) + (1 - f_{wet})/r_{cut} + f_{wet}/r_{ws}}. \tag{11}$$

Here r_b is the quasi-laminar boundary layer resistance over the leaf surface, which depends on molecular diffusivity and horizontal wind speed (Meyers, 1987), and r_{stm} is the stomatal resistance which is derived from the stomatal resistance for water vapour ($r_{stm,\mathrm{H_2O}}$) by a factor of the molecular diffusivity ratio,

$$r_{stm} = \frac{D_{\mathrm{H_2O}}}{D_{\mathrm{O_3}}} r_{stm,\mathrm{H_2O}}. \tag{12}$$

5 Here $D_{\mathrm{H_2O}}$ and $D_{\mathrm{O_3}}$ are the molecular diffusivities of water vapour and O_3, respectively. $r_{stm,\mathrm{H_2O}}$ is computed by SCADIS module in SOSAA and also used to calculate latent heat flux and thus the energy balance (Sogachev et al., 2002). r_{mes} (0 s m^{-1}) is the mesophyllic resistance which can be ignored for O_3. r_{cut} (10^5 s m^{-1}) is the cuticle resistance and r_{ws} (2000 s m^{-1}) represents the uptake on leaf wet skin. Their values are taken from Ganzeveld and Lelieveld (1995). Canopy wetness is represented by the fraction of wet skin f_{wet} which is determined by RH (Lammel, 1999; Wu et al., 2003),

10 $$f_{wet} = \begin{cases} 1 & 0.9 \leqslant \mathrm{RH} \\ \frac{\mathrm{RH}-0.7}{0.2} & 0.7 \leqslant \mathrm{RH} < 0.9 \\ 0 & \mathrm{RH} < 0.7 \end{cases}. \tag{13}$$

The threshold 70% is suggested by Altimir et al. (2006).

r_{ac} is the resistance representing the turbulent transport from the reference height of the understory vegetation to the soil surface. Since the gas transport is explicitly calculated in SOSAA and the bottom layer height is only ~ 0.3 m, the turbulence resistance between vegetation and ground is expected not to be an important factor for soil deposition, and consequently we

15 have set r_{ac} to zero. r_{bs} is the soil boundary layer resistance which is calculated as (Nemitz et al., 2000; Launiainen et al., 2013)

$$r_{bs} = \frac{\mathrm{Sc} - \ln(\delta_0/z_*)}{\kappa u_{*g}}. \tag{14}$$

Here Sc (1.07) is the Schmidt number for O_3. κ is the von Kármán constant (0.41). $\delta_0 = D_{\mathrm{O_3}}/(\kappa u_{*g})$ is the height above ground where the molecular diffusivity is equal to turbulent eddy diffusivity. z_* (0.1 m) is the height under which the logarithmic wind

20 profile is assumed. u_{*g} is the friction velocity near the ground. r_{soil} is the soil resistance, 400 s m^{-1} is used here according to Ganzeveld and Lelieveld (1995). A sensitivity analysis for r_{soil} will be shown in section 2.6. The diagram of the resistance analogy parametrisation method described above is shown in Fig. 1. All the symbols are also explained and listed in Table 4.

In the model the evolution of O_3 concentration is calculated for each layer by the prognostic equation

$$\frac{\partial [\mathrm{O_3}]}{\partial t} = \frac{\partial}{\partial z}\left(K_t \frac{\partial [\mathrm{O_3}]}{\partial z}\right) - V_d [\mathrm{O_3}] A + Q_{chem} \tag{15}$$

25 where the first term on the right-hand side represents the vertical mixing of O_3. The second term is the sink by dry deposition which is non-zero only inside the canopy. The last one is chemistry production and loss of O_3 for each model layer. V_d is the layer-specific conductance at height z which already includes the uptake by the leaves, including the leaf stomata and cuticle, as well as the uptake by the soil for the understory layer (Eq. 7). We have also distinguished the difference in uptake by dry and wet leaves. A is a unit scale factor which is set to 1 m^2 m^{-3} here. All the other chemical compounds are also computed
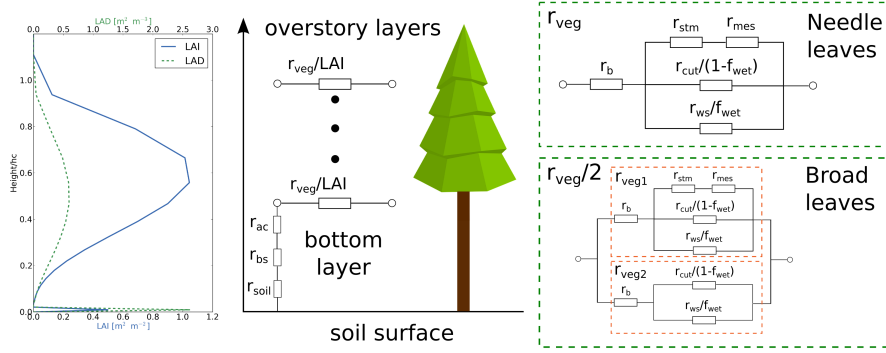
Figure 1. Vertical profiles of all-sided LAI (leaf area index) and LAD (leaf area density), as well as the diagram of resistance analogy method used in the O_3 dry deposition model. The overstory layers and the bottom layer are considered separately. The bottom layer includes the broad-leaved understory vegetation and soil surface. r_{ac} is the resistance representing the turbulent transport from the reference height of the understory vegetation to the soil surface. r_{bs} is the soil boundary layer resistance. r_{soil} is the soil resistance. r_b is the quasi-laminar boundary layer resistance above the leaf surface. r_{veg} represents the resistance to vegetation leaves, which is plotted on the right-hand side in details. For broad leaves, the resistance to the side with (r_{veg1}) or without (r_{veg2}) stomata is computed separately. r_{stm} is the stomatal resistance and r_{mes} is the mesophyllic resistance. r_{cut} is the cuticle resistance, r_{ws} is the resistance to wet skin. f_{wet} is the wet skin fraction. All the variables are defined for each layer. Note that here LAI is the all-sided leaf area index for each layer. The symbols are also explained in the text and Table 4.

following this prognostic equation. According to Eq. 3 the O_3 turbulent flux F_t in the model can be obtained as

$$F_t = -K_t \frac{\partial [O_3]}{\partial z}. \tag{16}$$

2.5 Model setup

In this study the newly implemented O_3 dry deposition module was applied to simulate the time period from Aug 1st to Aug 31st 2010 (Julian day 213 to 243). The model column domain was set from 0 m at ground surface up to 3000 m with 51 layers logarithmically configured, including the whole planetary boundary layer and part of the free atmosphere on top of it. We also constrained the model with the site-specific vegetation cover properties as presented before in section 2.1. The overstory layers only included needle-leaved part of Scots pine trees above ~ 0.3 m. Below that there was the understory vegetation and ground surface. Since the understory consisted of vegetation with leaves instead of needles, the parametrisation method for the understory vegetation was considered the same as that for broad-leaved species. In order to secure a more accurate representation of canopy wetness which was also relevant to the calculation of the layer-specific conductance for O_3, RH values inside the canopy were calculated from the measured absolute humidity and simulated air temperature.

In addition, to secure a realistic simulation of O_3 in a column model like SOSAA we also forced the model's O_3 concentration at 23 m to resemble the observed value every time step, the O_3 concentration at other levels were then calculated by Eq. 15.
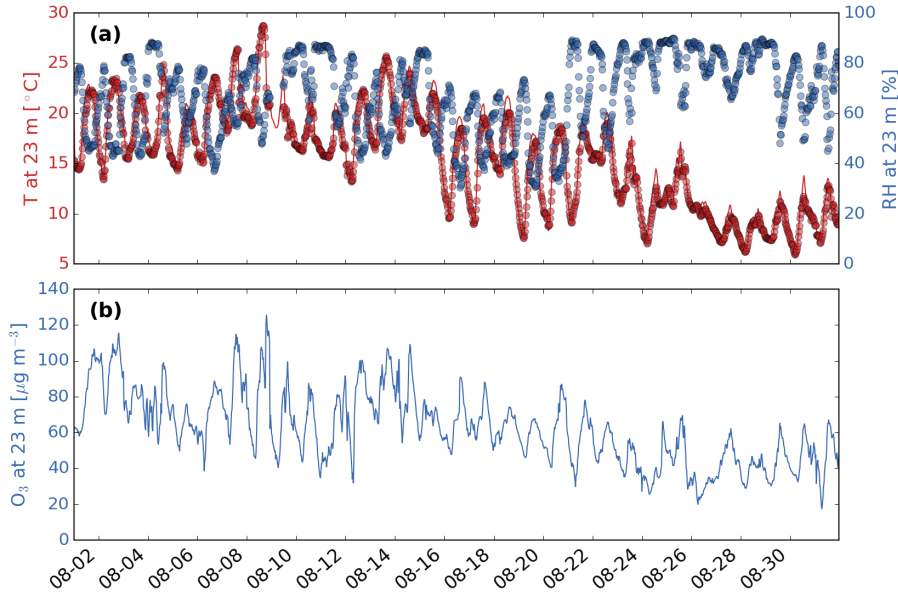
Figure 2. (a) Modelled (solid line) and measured (dots) time series of air temperature (T, red) and the measured ambient relative humidity (RH, blue) at 23 m above the ground. (b) Measured O_3 concentration (blue) at 23 m above the ground. The time period is August, 2010.

Table 1. Table of sensitivity cases. The case names and their short description texts are shown.

name	description
BASE	the same as described in section 2.4
RSOIL200	$r_{soil} = 200$ s m^{-1}
RSOIL600	$r_{soil} = 600$ s m^{-1}
RSOIL800	$r_{soil} = 800$ s m^{-1}
FREEO3	O_3 concentration at 23 m was also computed instead of using observed data

In this way, we implicitly added the role of advection in determining the O_3 concentration above the canopy. The gap-filled observed values which were used for the forcing are shown in Fig. 2b.

Several sensitivity cases have been conducted in this study (Table 1). In the case BASE all the parameters and methods were kept the same as described in section 2.4. In cases RSOIL200, RSOIL600 and RSOIL800 r_{soil} was altered to 200 s m^{-1}, 600 s m^{-1} and 800 s m^{-1}, respectively. In the case FREEO3, the O_3 concentration at 23 m was computed from Eq. (15) instead of being set to the measurement data.

Table 2. The average (MEAN) and standard deviation (STD) of modelled and measured O_3 fluxes (μg m^{-2} s^{-1}) above the canopy during different time periods (ALL for the whole month, D for daytime, N for nighttime) for different cases (OBS for measurement, BASE for basic settings used in this study, RSOIL200 uses the same settings as in BASE except $r_{soil} = 200$ s m^{-1}, similarly, RSOIL600 with $r_{soil} = 600$ s m^{-1} and RSOIL800 with $r_{soil} = 800$ s m^{-1}) are shown. The relative error (RE) of modelled O_3 flux compared to the observation $(F_{t,mod} - F_{t,obs})/F_{t,obs}$ is also listed within the parentheses.

CASES	ALL		D		N	
	MEAN±STD	RE	MEAN±STD	RE	MEAN±STD	RE
OBS	0.246 ± 0.175		0.334 ± 0.165		0.103 ± 0.073	
RSOIL200	0.286 ± 0.173	+16.4%	0.375 ± 0.162	+12.1%	0.140 ± 0.067	+35.0%
BASE	0.250 ± 0.153	+1.77%	0.329 ± 0.143	-1.74%	0.120 ± 0.059	+16.2%
RSOIL600	0.231 ± 0.144	-6.00%	0.305 ± 0.134	-8.85%	0.109 ± 0.057	+5.16%
RSOIL800	0.219 ± 0.139	-10.8%	0.290 ± 0.129	-13.2%	0.101 ± 0.055	-2.17%

2.6 Sensitivity analysis of r_{soil}

r_{soil} varied in different studies, ranging from 10 to 180 s m^{-1} for dry soil and 180 to 1100 s m^{-1} for wet soil (Massman, 2004). In this study the dry deposition module was developed on the basis of the model from Ganzeveld and Lelieveld (1995) in which r_{soil} was 400 s m^{-1}. In order to assess the uncertainties involved in estimating r_{soil}, different values of r_{soil} ranging from 200 to 800 s m^{-1} were tested in this study (Table 2). As can be expected, the modelled O_3 fluxes decreases as r_{soil} increases. The BASE case shows the best performance in general, although it overestimates $\sim$ 16% nighttime O_3 fluxes. Since the RSOIL200 case overestimates O_3 fluxes by $\sim$ 17% in average for the whole month, $\sim$ 12% at daytime and $\sim$ 35% at nighttime, the RSOIL200 sensitivity case indicates that using this lower estimate, a value that might be more appropriate for high organic (and dry) soils, seems not to represent properly the role of soil removal at this site. On the other hand, taking higher resistance values, e.g., one of 600 or 800 s m^{-1} seems to result in a better simulation of the role of the soil uptake at nighttime. However, considering the overall performance and better estimation of daytime O_3 fluxes, we used 400 s m^{-1} as the soil resistance in this study.

3 Results and discussion

3.1 Micrometeorology

The simulated month was warm and dry with little precipitation. Moreover, the temperature decreased dramatically in the middle of the month. In the first half of month (Aug 1st to Aug 15th) the average temperature at 23 m was 19.0 °C, while it dropped to 12.1 °C in the second half of month (Aug 16th to Aug 31st) (Fig. 2a). Analysis of the full temperature record indicated that this transition in the weather conditions at the site was well simulated by the model. RH varied inversely with
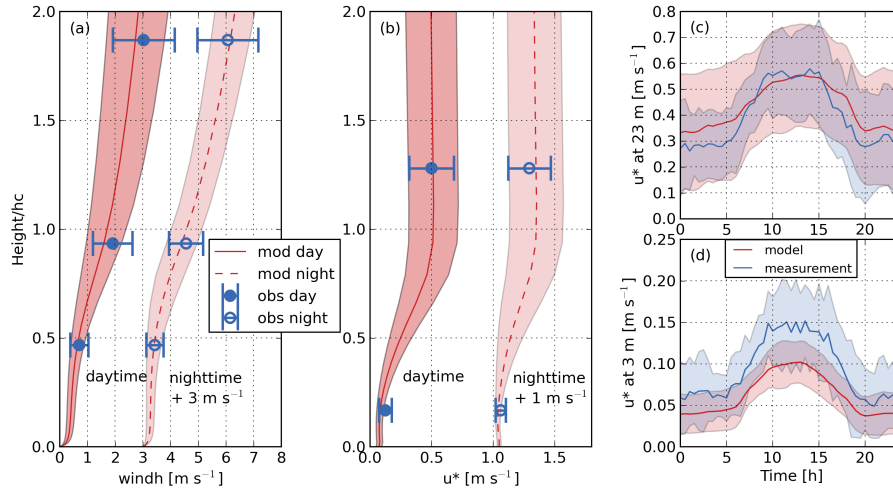
Figure 3. Modelled (red solid line for daytime, red dashed line for nighttime) and measured (blue solid circle for daytime, blue empty circle for nighttime) profiles of horizontal wind speed (windh) (a) and friction velocity ($u*$) (b). Nighttime values are shifted by 3 and 1 m s^{-1} for wind and $u*$ for clarity of presentation, respectively. The ranges of ± 1 standard deviation of modelled and measured data are marked as shades and error bars. The height is normalised by canopy height h_c. The monthly-mean diurnal cycles of modelled (red) and measured (blue) friction velocity at 23 m and 3 m are shown in (c) and (d). The ranges of ± 1 standard deviation are marked as shades in the same colours.

air temperature. Its average value increased only slightly from 66.0% in the first half of the month to 69.3% in the second half. However, a dramatic increase of daily mean RH values from 49.3% to 73.5% occurred between Aug 20th and Aug 21st (Fig. 2a). The combination of the dry weather and the large variation of temperature provided a good sample for verifying the O$_3$ dry deposition module.

5   Figure 3 shows the comparison results between simulated and measured horizontal wind speed and friction velocity (u_*). Both of them are essential for estimating the turbulent transport above and within the canopy as well as for the calculation of the quasi-laminar boundary layer resistance of leaves (r_b) at each canopy layer and the soil boundary layer resistance (r_{bs}). Figure 3a shows the good agreement between modelled and measured monthly-mean horizontal wind speed profiles during both daytime and nighttime. The wind speed decreases quickly inside the canopy due to canopy drag, then changes little below

10   0.5 h_c until near the surface where wind speed varies logarithmically to zero on the surface. The model reproduces the diurnal cycle of u_* but overestimates the nighttime values by ~ 0.05 m s^{-1} in average above the canopy (Fig. 3c). Below the canopy crown at ~ 3 m, u_* is underestimated by ~ 0.02 m s^{-1} at nighttime and ~ 0.05 m s^{-1} at daytime (Fig. 3d). The discrepancy is likely due to the limitation of representing the real heterogeneous dynamics by a 1D model with homogeneous canopy configuration.
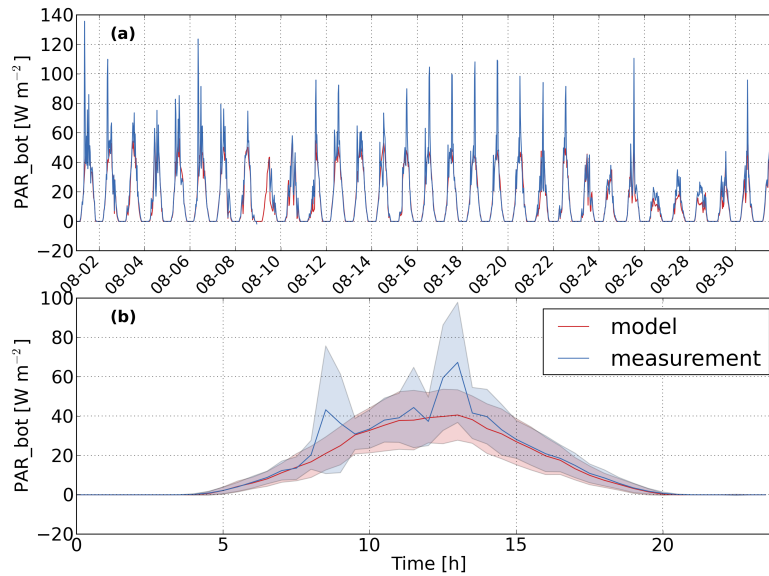
Figure 4. (a) Time series of PAR at 0.6 m from model (red) and measurement (blue) in August, 2010. (b) The monthly averaged diurnal cycle of time series in (a) for model (red) and measurement (blue). The range of ±1 standard deviation is marked by the shade with the same colour.

3.2 PAR above and below the canopy crown

Photosynthetically active radiation (PAR) plays an important role in stomatal exchange which determines to a large extent the daytime vegetation uptake. The PAR above the canopy is calculated directly from the measured incoming short wave radiation serving as input to the model, and shows a daytime maximum of about $250 - 300$ W m^{-2} during the simulation month. The
5   PAR inside the canopy is calculated by considering the absorption, reflection and scattering effects of canopy leaves in the model (Sogachev et al., 2002). The comparison between modelled and observed PAR at ~ 0.6 m below the canopy crown is shown in Fig. 4. The monthly-mean diurnal cycle of attenuated PAR below the canopy crown in the model is consistent with the observation except two missing peaks at daytime (Fig. 4b). These two peaks in the measurement are the consequence of direct exposure of PAR sensors to incoming solar radiation. Such situation always occurs when point-wise measurement is
10   compared with a model assuming a homogeneous forest canopy.

3.3 Energy balance

The monthly-mean diurnal cycles of sensible heat flux, latent heat flux, net radiation and soil heat flux, are shown in Fig. 5 in order to verify the simulated energy balance above the canopy in this study. The upward energy flux or the loss of surface energy is represented by positive values. During daytime, the soil and canopy loses energy by heat fluxes and gains energy mainly
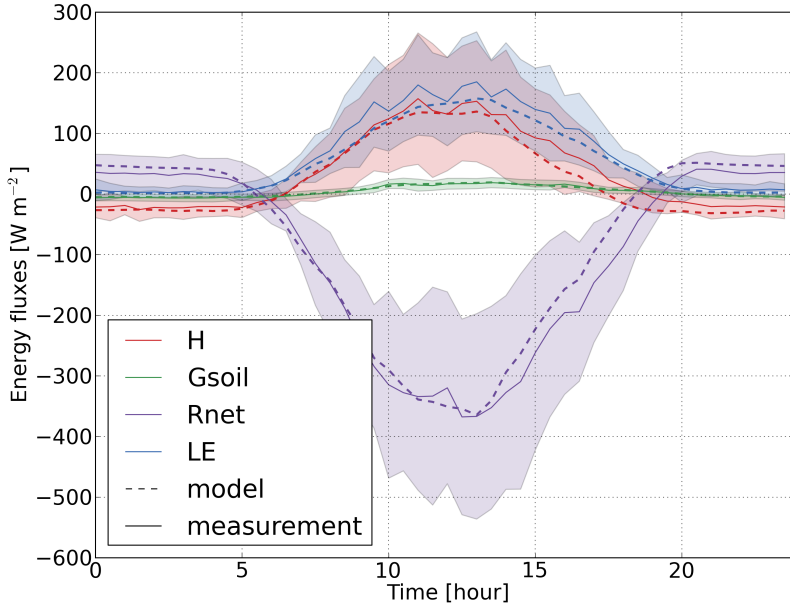
Figure 5. The monthly averaged diurnal cycle of different energy flux terms at 23 m above the ground for model (dashed lines) and measurement (solid lines), including sensible heat flux (H, red line), soil heat flux (Gsoil, green line), upward net radiation (Rnet, purple line, note the observed Rnet is at 67 m), latent heat flux (LE, blue line). The range of ± 1 standard deviation for measurement data is plotted for every term by the shade with the same colour.

from net incoming solar radiation. At night, the surface loses energy by net upward long wave radiation with an average rate of ~ 33 W m^{-2}, which is partly compensated by ~ 20 W m^{-2} downward energy from transport of warmer air.

During the simulation period the modelled diurnal cycles of energy fluxes agree well with the observation, although, for example, the latent heat flux is slightly underestimated by ~ 30 W m^{-2} during daytime. In the afternoon from 14:00 to 20:00 the sensible heat flux is underestimated by ~ 20 W m^{-2}. This could be explained by the underestimation in net radiation. However, the modelled values are generally within the one standard deviation range of the observations. The agreement between modelled and measured latent heat flux also indicates that the stomatal exchange, which controls the latent heat flux and is directly related to the stomatal resistance of O_3 and many other gaseous compounds, is realistically simulated as a function of the meteorological drivers.

3.4 O_3 fluxes

The modelled time series of O_3 turbulent flux and its diurnal cycle are compared with the measurement data above the canopy (Fig. 6). In general, the modelled flux shows a good agreement with the observations especially in the second half of month (Fig. 6a). Large discrepancies mostly occur in the first half of month which is warm and dry. On the first 3 days of the month,
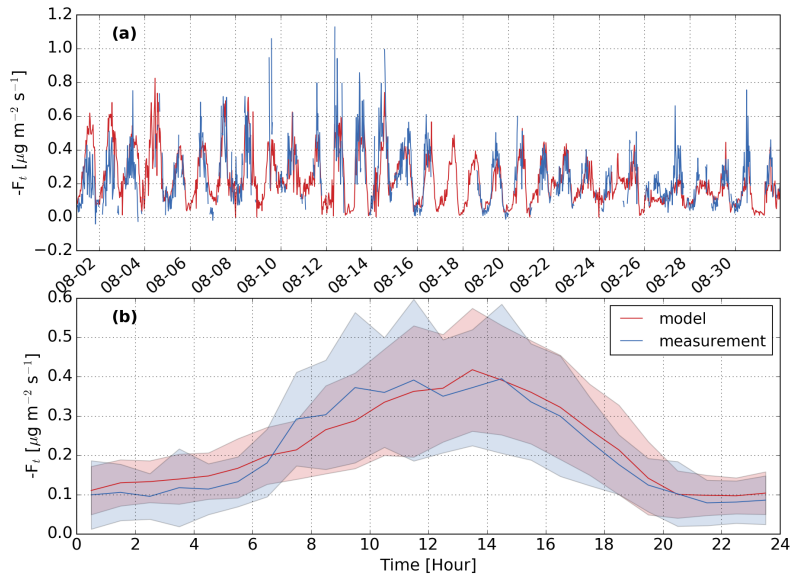
Figure 6. (a) Time series of the simulated (red) and measured (blue) O_3 turbulent fluxes above the canopy in August, 2010. (b) The monthly averaged diurnal cycles of time series presented in (a) for the model (red) and measurement (blue). The ranges of ± 1 standard deviation are marked by the shades with the same colours. Positive values represent downward fluxes.

the O_3 turbulent flux is overestimated by the model. At noon on some days (e.g., Aug 9th, 12th, 13th, 14th, 27th, 30th), the model is not able to predict the observed high peaks of O_3 turbulent fluxes. In an average diurnal cycle of O_3 turbulent flux, the model does not capture the rapid increase of downward O_3 turbulent flux in the morning, but it follows the measurement well after 10:00. In general the agreement between the simulated and measured monthly-mean diurnal cycles of O_3 turbulent

5 fluxes is promising.

Figure 7 shows the correlation between the simulated and measured O_3 turbulent fluxes above the canopy for different humidity conditions at daytime and nighttime separately. The overall R^2 between the modelled and measured O_3 turbulent fluxes for the whole dataset is 0.47. Among the four individual datasets under different conditions, the best prediction by the model occurs for the NH data points with R^2 of 0.37, followed by the results reflecting the daytime high humidity conditions

10 (R^2=0.19). Note that these conditions with highest correlations are also the conditions with high relative humidity, especially at nighttime. All the correlations are significant ($p < 0.001$) except the condition NL for which R^2 is only 0.02 (Fig. 7). This indicates the difficulty of simulating the O_3 turbulent flux in weak turbulent and low humidity conditions at nighttime. Rannik et al. (2009) revealed that the nighttime O_3 turbulent flux was affected by vertical advection of O_3. Therefore, when wet skin uptake is small for the condition NL, the vertical advection, which is not considered in the current model, could play a more

15 crucial role in O_3 turbulent flux than deposition. On the other hand, there are only 69 observed data points in the condition NL which implies larger random uncertainty. However, when the surface is wetter, the simulated nocturnal O_3 turbulent fluxes
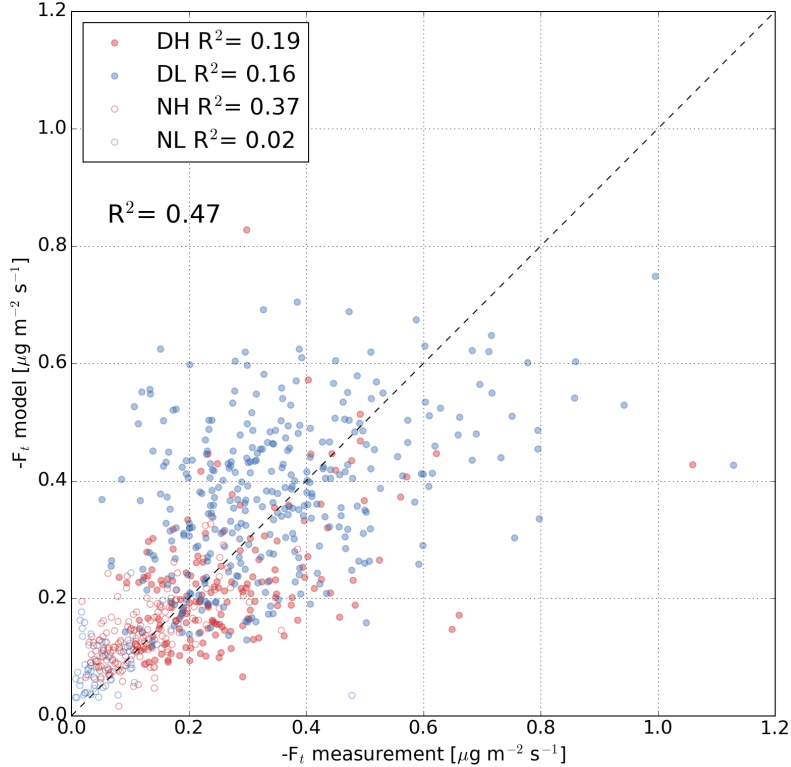
Figure 7. Scatter plots of modelled versus measured O_3 turbulent fluxes above the canopy. The data points are plotted separately for different groups (DH, DL, NH and NL) with their R^2 values shown in the legend. R^2 of the whole dataset is shown below the legend.

correlates much better with the measurement. In addition, the measurement data shows a larger range of variation (about -1.2 – 0.0 μg m^{-2} s^{-1}) compared to the range in the modelled O_3 turbulent flux (about -0.8 – 0.0 μg m^{-2} s^{-1}), which implies that the model does not capture the O_3 turbulent flux peaks or the measurements are more scattered due to random errors. Regarding the low R^2 values here, we should consider the uncertainty of measured fluxes. Such uncertainty contributes to the

5   data scattering when comparing the modelled and measured fluxes, such as in Fig. 7, and reduces the correlation statistics.

In general, the parametrisation of wet skin fraction (Eq. (13)) and its impact on O_3 non-stomatal removal seems to represent the O_3 deposition mechanisms inside the canopy well considering the good performance under high humidity conditions. Although the prediction of O_3 turbulent flux with weak turbulence at night under low humidity condition still has large uncertainties (Fig. 7), the simulated average nocturnal O_3 turbulent flux above the canopy shows a good agreement with the

10   observation (Fig. 6b).

3.5 O$_3$ concentration profile

In order to evaluate if the good agreement between the observed and simulated O$_3$ turbulent fluxes above the canopy also implies a realistic representation of the O$_3$ concentration inside the canopy, we have conducted an evaluation of the simulated in-canopy O$_3$ concentration profile. The one-month averaged O$_3$ concentration profiles from model results and measurements are shown in Fig. 8. The huge variation range results from the meteorological variations in this month, especially the dramatic transition in the middle of the month (Fig. 2). The average O$_3$ concentration of the whole month is 60.4 μg m^{-3} at 23 m, then decreases gradually inside the canopy to 54.1 μg m^{-3} at 4.2 m due to the in-canopy sinks, which are most likely dominated by deposition. Similar vertical gradients are also found for the four different conditions. At night, the turbulent mixing is smaller compared to daytime which inhibits the downward transport of air mass with larger concentration of O$_3$ into the canopy. Hence the O$_3$ removal by canopy and especially by soil surface results in larger gradient of O$_3$ inside the canopy during nighttime (Fig. 8).

The model results of O$_3$ concentration profiles show a good agreement with the observations except the slight overestimation for the DH condition below $\sim$ 8 m (0.45 h_c) and the apparent underestimation for the NL condition throughout the whole canopy. This is consistent with the model results of the O$_3$ turbulent fluxes, which shows $\sim$ 20% underestimation for the DH condition and $\sim$ 38% overestimation for the NL condition. In addition, the modelled vertical gradient of O$_3$ concentration during nighttime at drier conditions (NL) is much larger inside the canopy compared to the measured gradient, which implies that the soil deposition is largely overestimated when the soil and dry vegetation surface uptake dominates the overall removal inside the canopy. This also indicates that further investigation is needed for the more precise representation of ground surface deposition at different humidity conditions, including possibly the roles of uptake by the moss layer and soil humus layer.

3.6 O$_3$ flux profile

The normalised cumulative O$_3$ deposition flux at layer i can be obtained as

$$F_{c,i} = \frac{\sum_{k=1}^{i} F_k}{\sum_{k=1}^{N} F_k} \tag{17}$$

where F_k is the O$_3$ deposition flux at layer k and N is the layer index just above the canopy. The profiles of F_c and the contributions of different deposition pathways for four different conditions are shown in Fig. 9. For the whole month, the O$_3$ uptake is dominated by soil deposition below 0.2 h_c ($\sim$ 3.6 m) with only $\sim$ 8% contribution from the understory vegetation via stomatal uptake. From 0.2 h_c to 0.8 h_c ($\sim$ 14.4 m) the cumulative uptake on leaf surfaces increases with height due to dense leaves in the plant crown area. Above 0.8 h_c there only remains small portion of biomass ($\sim$ 7%) providing less than 2% O$_3$ uptake compared to the total O$_3$ deposition.

The soil uptake contributes to the total O$_3$ deposition flux at both daytime and nighttime (Figs. 9b and 9c) with a percentage of $\sim$ 32% and $\sim$ 54%, respectively. At daytime, $\sim$ 63% of the O$_3$ deposition flux is due to stomatal uptake. While at nighttime, when RH is larger than 70% at most of the time, the cumulative wet skin uptake contributes $\sim$ 41% to the total O$_3$ deposition. At nighttime under high humidity conditions, the wet skin uptake even contributes $\sim$ 51% to the total O$_3$ deposition fluxes
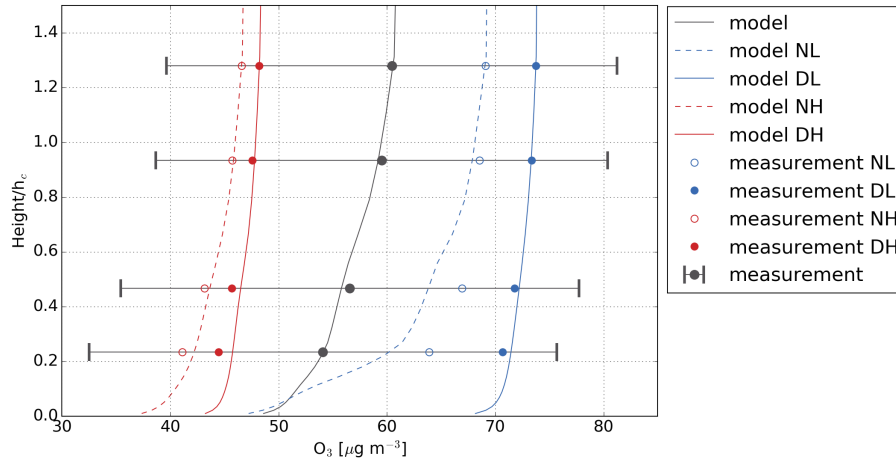
Figure 8. Measured average vertical profiles of O_3 concentration for the whole month (dark grey, the horizontal bars are ± 1 standard deviations) and individual conditions (daytime under high humidity condition, labelled as DH with red filled circle; daytime under low humidity condition, labelled as DL with blue filled circle; nighttime under high humidity condition, labelled as NH with red empty circle; nighttime under low humidity condition, labelled as NL with blue empty circle). Modelled results are plotted as solid lines (daytime) and dashed lines (nighttime) with the same colour as measurement. The height is normalised by the canopy height h_c.

(Table 3). This indicates that wet skin uptake relevant to RH plays a crucial role at night which is consistent with the results in Rannik et al. (2012). As a result, the simulated averaged non-stomatal contribution to the integrated O_3 deposition flux above the canopy is $\sim 37\%$ during daytime and $\sim 96\%$ during nighttime (Table 3). It should be noted that the stomata are not completely closed at night (Caird et al., 2007) and the minimum stomatal conductance at nighttime is about 5% of its maximum
5   value at daytime (Kolari et al., 2007) which is similar with the simulation result here ($3.7\%/63.0\% \approx 6\%$, Table 3).

Above $0.2\ h_c$, the stomatal uptake (DL, Fig. 9b), wet skin uptake (NH, Fig. 9c) or both of them (DH, Fig. 9a; NL, Fig. 9d) start to play a significant role in the cumulative O_3 deposition fluxes. Hence at $0.8\ h_c$ the cumulative contribution of soil deposition is less than 50% except in the NL condition when both the cumulative stomatal uptake and wet skin uptake are limited. In all the four conditions the dry cuticle uptake is minor with a maximum contribution of about 5.0% for the NL
10   condition.

During daytime the sub-canopy layer including soil surface, contributes about 38% to the integrated O_3 deposition, which is consistent with the results from Launiainen et al. (2013) in which the sub-canopy (lower than 4.2 m) contribution was 35–45% at daytime. At night the contribution increases to around 60% due to the closed stomata in crown layers. This is much higher than that (25 – 30%) in Launiainen et al. (2013) (Table 3). The overestimation could result from the underestimation of
15   the soil resistance, which is difficult to determine in such a complex ground ecosystem. However, among these four different conditions with the same constant soil uptake efficiency, only under the nocturnal dry conditions (NL) there is apparently an overestimation in O_3 uptake and consequently underestimation of the O_3 concentration inside the canopy (Fig. 8). Therefore,
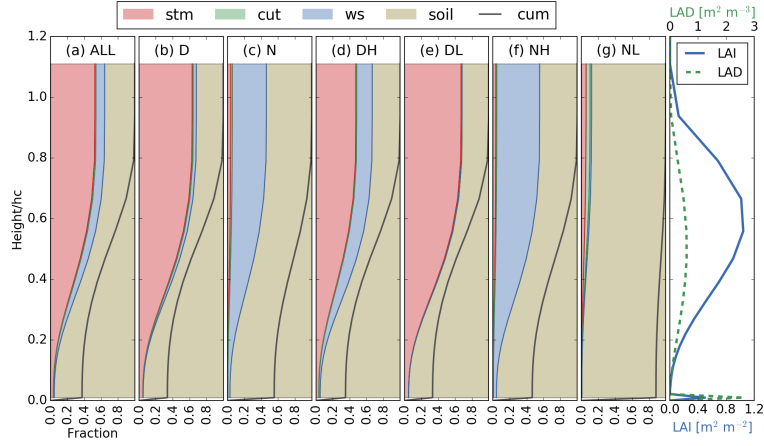
Figure 9. Simulated vertical profiles of cumulative O_3 deposition flux normalised by the integrated O_3 deposition flux above the canopy (cum, solid black line) for four conditions DH (a), DL (b), NH (c) and NL (d). D and N represent daytime and nighttime, H and L represent high and low humidity, respectively. Shaded areas are the cumulative contribution fractions for different deposition pathways, including stomatal uptake (stm, red), cuticle uptake (cut, green), wet skin uptake (ws, blue) and soil uptake (soil, pale brown). The all-sided LAI profile for each layer and LAD is plotted again here (e). The height is normalised by the canopy height h_c.

Table 3. The first four columns are the contribution fractions of different deposition pathways (stm as stomatal uptake, wet as wet skin uptake, cut as cuticle uptake, soil as soil surface uptake) in the integrated O_3 deposition flux inside the canopy in the model. The last column is the sub-canopy (below 4.2 m) O_3 turbulent flux ($F_{t,mod}(4.2m)$) compared to the O_3 turbulent flux above the canopy ($F_{t,mod}$) in the model. Different conditions are listed along the row. D and N represent daytime and nighttime, H and L represent high and low humidity, respectively. ALL is for the whole dataset.

	stm	wet	cut	soil	$F_{t,mod}(4.2m)/F_{t,mod}$
D	63.0%	3.79%	1.12%	32.1%	38.0%
N	3.70%	40.5%	1.87%	53.9%	59.5%
DH	47.2%	18.5%	0.94%	33.4%	39.6%
DL	67.1%	0.00%	1.17%	31.8%	37.6%
NH	3.28%	51.0%	1.04%	44.7%	51.4%
NL	5.42%	1.78%	4.73%	88.1%	89.5%
ALL	52.5%	10.4%	1.25%	35.8%	41.7%

we expect that the poor performance for the NL condition also results from the limited data amount under this condition (only 69 data points) which leads to larger ratio of random uncertainty and thus smaller R^2.

Moreover, the assumption that the resistance r_{ac} between the understory vegetation and ground is not a limiting factor for soil deposition might not hold under certain conditions. On the other hand, Launiainen et al. (2013) studied one month earlier (July 1st to August 4th, 2010) than the time period (August 1st to August 31st, 2010) in this study, so the difference between these two studies could also be due to the meteorological and biological variations during the two summer months. However, the daytime contribution of the sub-canopy layer is consistent, so the difference between the two months could only play a minor effect.

3.7 Contribution of air chemistry

The role of chemical processes in explaining the O_3 removal inside the forest canopy have been discussed in previous studies (e.g., Altimir et al., 2006; Wolfe et al., 2011; Rannik et al., 2012; Launiainen et al., 2013). A study by Wolfe et al. (2011) found that the non-stomatal uptake over a Ponderosa pine stand in the US was associated with additional very reactive BVOCs being present besides the identified ones. On the other hand, Rannik et al. (2012) suggested that the air chemistry provided only minor contribution at SMEAR II. In order to estimate the contribution of chemical removal at SMEAR II, two different studies applied multi-layer models (Rannik et al., 2012; Launiainen et al., 2013) to simulate the O_3 fluxes and concentration inside the boreal forest canopy. However, both of them showed their limitations on estimating the chemical contribution. Rannik et al. (2012) only considered one chemical reaction of O_3 with β-caryophyllene. While in Launiainen et al. (2013), they simplified the chemical production and loss of O_3 with only two parameters to represent the first-order kinetic sink and photo-chemical production. In this study, we implemented a chemistry module with a detailed list of chemical reactions (see section 2.4.1), which was able to provide a more accurate estimation of chemical removal of O_3 inside the canopy.

In order to get rid of the effect of synoptic-scale transport of O_3 and only focus on the local sinks and sources, we applied the simulation case FREEO3. In this simulation case we ignored the role of advection and only considered the role of local sources and sinks inside the canopy, i.e., dry deposition, chemical production and loss, and turbulent transport. Here the time period from Aug. 5th to 14th were selected from the simulation results to analyse the local chemical contribution, because the modelled O_3 concentration fitted to the measurement the best during this period out of the whole month for the case FREEO3, which indicated that the advection also did not have apparent effect on the local observed O_3 variation. The daily averaged (from Aug. 5th to 14th) production and loss of O_3 inside the canopy caused by dry deposition (F_{depo}) and chemistry (F_{chem}) are plotted in Fig. 10. The unit μg m^2 s^{-1} means how much μg O_3 inside the canopy alters per unit square meter per second. So positive values correspond to O_3 production and negative values represent O_3 loss. Here the chemistry production is a net effect of O_3 loss reactions and photo-chemical production. F_{depo} (obviously negative) shows a maximum O_3 loss rate at about 14:00. While the chemistry produces O_3 from morning at $\sim$ 06:00 to the afternoon at $\sim$ 15:00, and destroys it throughout the other time of the day, especially at nighttime (Fig. 10). The ratio between F_{chem} and F_{depo} shows that chemical removal has its largest contribution of $\sim$ 9% of the dry deposition sink in average at nighttime from 20:00 to 04:00. At daytime, our model simulation indicates that the O_3 production caused by chemistry can compensate up to $\sim$ 4% of dry deposition loss in average. However, during the selected period, the chemical contribution and compensation can reach up to $\sim$ 24% and $\sim$ 20% at most.
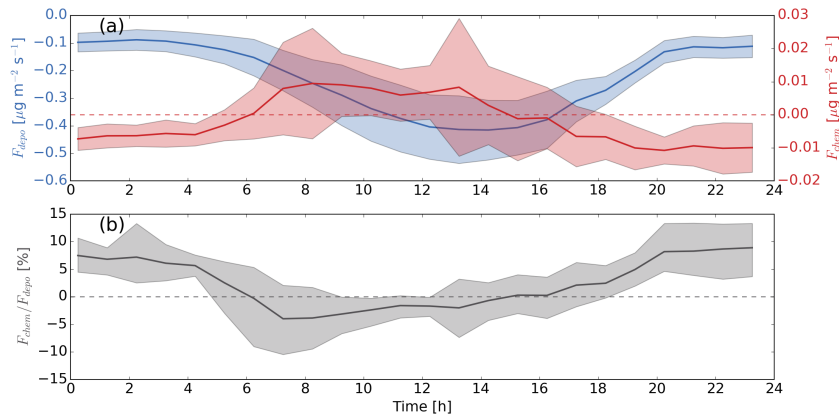
Figure 10. (a) The daily averaged (from Aug. 5th to 14th) production and loss caused by chemistry (F_{chem}, red) and dry deposition (F_{depo}, blue). (b) The ratio between F_{chem} and F_{depo}. Zero lines for F_{chem} and the ratio are plotted as dashed lines. Shaded areas show the range of ± 1 standard deviation.

This indicates that in general chemistry has minor impact on O_3 alteration, but at some specific time the chemical production and removal of O_3 can still play a significant role.

As a comparison, we also calculated the time scales of different removal processes to estimate the contribution of air chemistry. The average value of measured O_3 flux ($F_{O_3,avg}$) in August, 2010 above the canopy was 0.33 μg m^{-2} s^{-1} at daytime and 0.10 μg m^{-2} s^{-1} at nighttime whereas the O_3 concentration ($[O_3]$) inside the canopy was about 61.6 μg m^{-3} during daytime and 50.5 μg m^{-3} at night on average. So the time scale of total O_3 flux (τ_{O_3}) could be obtained from

$$\tau_{O_3} = [O_3] \, h_c / F_{O_3,avg} \tag{18}$$

which was ~ 3400 s (~ 1 h) for daytime and ~ 9100 s (~ 2.5 h) for nighttime. On the other hand, the total O_3 reactivity (y) at 18 m during a similar time period and at the same boreal forest station was calculated by Mogensen et al. (2015), which was 1.58×10^{-5} s^{-1} and 1.67×10^{-5} s^{-1} for noon and 2 a.m. at night. If the same values were assumed to be applicable also inside the canopy, the time scale of the O_3 removal by chemistry (τ_{c,O_3}) was

$$\tau_{c,O_3} = y^{-1} \tag{19}$$

which was ~ 63300 s (~ 18 h) for daytime and ~ 59900 s (~ 17 h) for nighttime. These estimates showed that the chemical removal accounted for about 5% (3400/63300) and 15% (9100/59900) of the total O_3 removal within the canopy at daytime and nighttime, respectively.

Compared to the simulation results, the time scale analysis could not reflect the photochemical production of O_3 during daytime, hence the estimation of net chemical effects is not possible with this method. For nighttime, the time scale analysis overestimates the average contribution of chemical removal by about 88% (15% compared to 8%, 8% is obtained from

9%/(100%+9%)). The comparison result could act as a proof of the statement in Wolfe et al. (2011), which argued that the time scale might not be a good criteria of chemical influence.

4 Summary

A detailed multi-layer O_3 dry deposition model has been implemented into SOSAA to investigate the O_3 uptake by canopy and soil surface at a boreal forest station SMEAR II. The presented detailed analysis of the O_3 deposition processes for this site also quantified various removal processes, e.g., by the dry and wet cuticle, by stomatal uptake and by the soil surface.

In this model the fraction of wet skin on canopy leaves was parametrised according to RH values to analyse the potential role of canopy wetness on O_3 deposition for both high and low humidity conditions. Moreover, the multi-layer model also enabled the study of deposition processes inside the canopy and the partitioning of O_3 deposition fluxes between the canopy crown and sub-canopy. In this study, the model has been validated by comparing the modelled and measured O_3 turbulent flux above the canopy and its concentration profile inside the canopy.

Further investigation has been done through a more in-depth correlation analysis on O_3 turbulent fluxes for nighttime and daytime under high and low humidity conditions. The simulated O_3 turbulent fluxes above the canopy correlated reasonably well with the measurement for the whole month with R^2 of 0.47 ($p < 0.001$), which was also consistent with the plausible prediction of O_3 concentration profile inside the canopy. The significant correlation ($p < 0.001$) also applied to the daytime humid and dry as well as nighttime humid conditions (DH, DL and NH) with R^2 of 0.19, 0.16 and 0.37. However, the model was not able to predict high peaks with O_3 turbulent fluxes larger than 0.8 μg m^{-2} s^{-1}. The model also did not capture well the measured O_3 removal for the nocturnal dry condition (NL), in which R^2 was only 0.02 and the O_3 concentration inside the canopy was largely underestimated (Figs. 7 and 8). The possible reasons could be the limited data amount implying larger random uncertainty.

Nearly all of the O_3 uptake occurred below 0.8 h_c inside the canopy. During daytime, the contributions of stomatal uptake ($\sim$ 47%), wet skin uptake ($\sim$ 19%) and soil uptake ($\sim$ 33%) were significant for the total O_3 uptake under high humidity conditions. While under low humidity conditions the stomatal ($\sim$ 67%) and soil uptake (32%) contributed dominantly the overall canopy deposition. During nighttime, the stomatal uptake contribution ($\sim$ 3%) was not zero, but was much smaller compared to the wet skin uptake ($\sim$ 51%) under high humidity conditions. For the low humidity condition at night, nearly all the deposition ($\sim$ 88%) was due to soil uptake. Since RH was larger than 70% at most of the time during night, the uptake by wet canopy could be a dominant factor for the nocturnal O_3 removal. In addition, the simulated non-stomatal contributions to the integrated O_3 deposition fluxes were estimated as about 53%, 33%, 97% and 95% for conditions DH, DL, NH and NL, respectively (Table 3).

The modelled contribution of sub-canopy deposition during daytime ($\sim$ 38%) was consistent with that (35 − 45%) in Launiainen et al. (2013), but it was much higher at nighttime ($\sim$ 60%) compared to that in the same study (25 − 30%) (Table 3). This discrepancy at nighttime was most likely due to the overestimation of soil uptake.

The contribution of O_3 removal by chemical reactions with currently identified BVOCs have also been evaluated. In general the air chemistry played a minor role in O_3 uptake inside the canopy. In the simulated averaged diurnal cycle, the air chemistry produced O_3 during daytime from about 06:00 to 15:00, compensating up to 4% of dry deposition sinks. While at nighttime, the chemical loss enhanced O_3 removal by $\sim 9\%$ of that by dry deposition. A qualitative estimation of chemical contribution with time scale analysis was also conducted as a comparison. However, this method overestimated the air chemical removal by about 88% for nighttime and it was not able to reflect the O_3 production at daytime.

This study is the first step to establish a detailed gas dry deposition model in SOSAA. Further analysis of dry deposition will be done for other chemical compounds, especially for BVOCs. This will improve not only the ability to simulate air chemistry and aerosol processes but also our understanding of the mechanisms involved in the removal processes at boreal forest. In addition, it is also of scientific interest to investigate how future climate change might ultimately affect the removal processes of compounds like O_3 and BVOCs for boreal forests.

Appendix A: Table of symbols

Table 4: Table of symbols

symbol	value	unit	description
h_c	18	m	canopy height
LAI		$m^2 \, m^{-2}$	all-sided leaf area index at each layer
T		K	air temperature
q_v		$kg \, m^{-3}$	specific humidity
RH		-	relative humidity
X		-	scalar quantity
u_*		$m \, s^{-1}$	friction velocity
u_{*g}		$m \, s^{-1}$	friction velocity near the ground
H		$W \, m^{-2}$	sensible heat flux
LE		$W \, m^{-2}$	latent heat flux
$F_{t,X}$		-	turbulent flux of X
F_t		$\mu g \, m^{-2} \, s^{-1}$	O_3 turbulent flux
K_t		$m^2 \, s^{-1}$	turbulent eddy diffusivity
K_h		$m^2 \, s^{-1}$	turbulent eddy diffusivity for heat fluxes
TKE		$m^2 \, s^{-2}$	turbulent kinetic energy
ε		$m^2 \, s^{-3}$	dissipation rate of TKE
ω		s^{-1}	specific dissipation of TKE
$C_{p,air}$	1009.0	$J \, kg^{-1} \, K^{-1}$	latent heat flux

symbol	value	unit	description
ρ_{air}	1.205	kg m^{-3}	air density
γ_d	0.0098	K m^{-1}	lapse rate of dry air
L_v	2.256×10^6	J kg^{-1}	latent heat of vapourisation for water
C_μ	0.0436	-	closure constant in calculating K_t
A	1	m^2 m^{-3}	a scale factor
Q_{chem}		μg m^{-3} s^{-1}	chemical production and loss
F		μg m^{-2} s^{-1}	O$_3$ deposition flux
[O$_3$]		μg m^{-3}	O$_3$ concentration
V_d		m s^{-1}	layer-specific conductance for O$_3$
r_{veg}		s m^{-1}	leaf surface resistance
r_{veg1}		s m^{-1}	leaf surface resistance to the side without stomata
r_{veg2}		s m^{-1}	leaf surface resistance to the side with stomata
r_b		s m^{-1}	quasi-laminar boundary layer resistance over leaf surface
r_{ac}	0	s m^{-1}	resistance of turbulent transport from the reference height of the understory vegetation to the soil surface
r_{bs}		s m^{-1}	soil boundary layer resistance
r_{soil}	400	s m^{-1}	soil resistance
r_{stm}		s m^{-1}	stomatal resistance
$r_{stm,\mathrm{H_2O}}$		s m^{-1}	stomatal resistance for water vapour
r_{mes}	0	s m^{-1}	mesophyllic resistance
r_{cut}	10^5	s m^{-1}	cuticle resistance
r_{ws}	2000	s m^{-1}	wet skin resistance
f_{wet}		-	fraction of wet skin
$D_{\mathrm{H_2O}}$	2.12×10^{-5}	m^2 s^{-1}	molecular diffusivity of water vapour
$D_{\mathrm{O_3}}$	1.33×10^{-5}	m^2 s^{-1}	molecular diffusivity of O$_3$
κ	0.41	-	von Kármán constant
δ_0		m	the height above ground where the molecular diffusivity is equal to turbulent eddy diffusivity
z_*	0.1	m	the height under which the logarithmic wind profile is assumed
Sc	1.07	-	Schmidt number for O$_3$

Author contributions. Putian Zhou implemented the deposition code into SOSAA, made the simulation runs, analysed the results and wrote the main part of this manuscript. Laurens Ganzeveld provided and developed the deposition code, suggested the concepts of manuscript structure, contributed the micrometeorology part and the discussions related to O$_3$ fluxes. Üllar Rannik contributed the micrometeorology

part, the discussions related to O_3 flux measurements and the discussions in chemical removal processes. Luxi Zhou contributed implementing the deposition code into SOSAA and configuration of simulation runs. Rosa Gierens contributed the configuration of meteorology part in SOSAA and configuration of simulation runs. Ditte Taipale contributed the discussions related to air chemistry and site description. Ivan Mammarella contributed discussions related to O_3 flux measurements. Michael Boy provided SOSAA code and the main concept and structure of this manuscript.

Acknowledgements. This work was supported by Maj ja Tor Nessling funding, the Academy of Finland (projects 1118615 and 272041), CRAICC (Cryosphere-atmosphere interactions in a changing Arctic climate), eSTICC (eScience tools for investigating Climate Change in Northern High Latitudes) and FCoE (The Centre of Excellence in Atmospheric Science - From Molecular and Biological processes to The Global Climate). This work was also supported by institutional research funding (IUT20-11) of the Estonian Ministry of Education and Research, and the European Regional Development Fund (Centre of Excellence EcolChange). The authors also wish to acknowledge CSC - IT Center for Science, Finland, for computational resources.

References

Altimir, N., Kolari, P., Tuovinen, J.-P., Vesala, T., Bäck, J., Suni, T., Kulmala, M., and Hari, P.: Foliage surface ozone deposition: a role for surface moisture?, Biogeosciences, 3, 209–228, 2006.

Boy, M., Sogachev, A., Lauros, J., Zhou, L., Guenther, A., and Smolander, S.: SOSA–a new model to simulate the concentrations of organic vapours and sulphuric acid inside the ABL – Part 1: Model description and initial evaluation, Atmos. Chem. Phys., 11, 43–51, 2011.

Boy, M., Mogensen, D., Smolander, S., Zhou, L., Nieminen, T., Paasonen, P., Plass-Dülmer, C., Sipilä, M., Petäjä, T., Mauldin, L., Berresheim, H., and Kulmala, M.: Oxidation of SO_2 by stabilized Criegee intermediate (sCI) radicals as a crucial source for atmospheric sulfuric acid concentrations, Atmospheric Chemistry and Physics, 13, 3865–3879, doi:10.5194/acp-13-3865-2013, http://www.atmos-chem-phys.net/13/3865/2013/, 2013.

Bäck, J., Aalto, J., Henriksson, M., Hakola, H., He, Q., and Boy, M.: Chemodiversity of a Scots pine stand and implications for terpene air concentrations, Biogeosciences, 9, 689–702, 2012.

Caird, M. A., Richards, J. H., and Donovan, L. A.: Nighttime Stomatal Conductance and Transpiration in C_3 and C_4 Plants, Plant Physiology, 143, 4–10, 2007.

Dee, D. P., Uppala, S. M., Simmons, A. J., Berrisford, P., Poli, P., Kobayashi, S., Andrae, U., Balmaseda, M. A., Balsamo, G., Bauer, P., Bechtold, P., Beljaars, A. C. M., van de Berg, L., Bidlot, J., Bormann, N., Delsol, C., Dragani, R., Fuentes, M., Geer, A. J., Haimberger, L., Healy, S. B., Hersbach, H., Hólm, E. V., Isaksen, L., Kållberg, P., Köhler, M., Matricardi, M., McNally, A. P., Monge-Sanz, B. M., Morcrette, J.-J., Park, B.-K., Peubey, C., de Rosnay, P., Tavolato, C., Thépaut, J.-N., and Vitart, F.: The ERA-Interim reanalysis: configuration and performance of the data assimilation system, Quarterly Journal of the Royal Meteorological Society, 137, 553–597, doi:10.1002/qj.828, http://dx.doi.org/10.1002/qj.828, 2011.

Fares, S., McKay, M., Holzinger, R., and Goldstein, A. H.: Ozone fluxes in a Pinus ponderosa ecosystem are dominated by non-stomatal processes: Evidence from long-term continuous measurements, Agricultural and Forest Meteorology, 150, 420–431, 2010.

Felzer, B. S., Cronin, T., Reilly, J. M., Melillo, J. M., and Wang, X.: Impacts of ozone on trees and crops, Comptes Rendus Geoscience, 339, 784–798, 2007.

Ganzeveld, L. and Lelieveld, J.: Dry deposition parameterization in a chemistry general circulation model and its influence on the distribution of reactive trace gases, J. Geophy. Res., 100, 20 999–21 012, 1995.

Ganzeveld, L., Lelieveld, J., and Roelofs, G.-J.: A dry deposition parameterization for sulfur oxides in a chemistry and general circulation model, Journal of Geophysical Research: Atmospheres, 103, 5679–5694, doi:10.1029/97JD03077, http://dx.doi.org/10.1029/97JD03077, 1998.

Ganzeveld, L., Bouwman, L., Stehfest, E., van Vuuren, D. P., Eickhout, B., and Lelieveld, J.: Impact of future land use and land cover changes on atmospheric chemistry-climate interactions, Journal of Geophysical Research: Atmospheres, 115, n/a–n/a, doi:10.1029/2010JD014041, http://dx.doi.org/10.1029/2010JD014041, d23301, 2010.

Ganzeveld, L. N., Lelieveld, J., Dentener, F. J., Krol, M. C., Bouwman, A. J., and Roelofs, G.-J.: Global soil-biogenic NOx emissions and the role of canopy processes, Journal of Geophysical Research, 107, ACH 9–1–ACH 9–17, doi:10.1029/2001JD001289, http://dx.doi.org/10.1029/2001JD001289, 2002a.

Ganzeveld, L. N., Lelieveld, J., Dentener, F. J., Krol, M. C., and Roelofs, G.-J.: Atmosphere-biosphere trace gas exchanges simulated with a single-column model, Journal of Geophysical Research, 107, ACH 8–1–ACH 8–21, doi:10.1029/2001JD000684, http://dx.doi.org/10.1029/2001JD000684, 2002b.

Gierens, R. T., Laakso, L., Mogensen, D., Vakkari, V., Beukes, J. P., Van Zyl, P. G., Hakola, H., Guenther, A., Pienaar, J. J., and Boy, M.: Modelling new particle formation events in the South African savannah, South African Journal of Science, doi:10.1590/ sajs.2014/20130108, 2014.

Goldstein, A. H., McKay, M., Kurpius, M. R., Schade, G. W., Lee, A., Holzinger, R., and Rasmussen, R. A.: Forest thinning experiment confirms ozone deposition to forest canopy is dominated by reaction with biogenic VOCs, Geophysical Research Letters, 31, n/a–n/a, doi:10.1029/2004GL021259, http://dx.doi.org/10.1029/2004GL021259, l22106, 2004.

Guenther, A. B., Karl, T., Harley, P., Wiedinmyer, C., Palmer, P. I., and Geron, C.: Estimates of global terrestrial isoprene emissions using MEGAN(Model of Emissions of Gases and Aerosols from Nature), Atmos. Chem. Phys., 6, 3181–3210, 2006.

Hardacre, C., Wild, O., and Emberson, L.: An evaluation of ozone dry deposition in global scale chemistry climate models, Atmos. Chem. Phys., 15, 6419–6436, 2015.

Hari, P. and Kulmala, M.: Station for Measuring Ecosystem-Atmosphere Relations (SMEAR II), Boreal. Environ. Res., 10, 315–322, 2005.

Junninen, H., Lauri, A., Keronen, P., Aalto, P., Hiltunen, V., Hari, P., and Kulmala, M.: Smart-SMEAR: on-line data exploration and visualization tool for SMEAR stations, Boreal Environment Research, 14, 447–457, 2009.

Kampa, M. and Castanas, E.: Human health effects of air pollution, Environmental Pollution, 151, 362–367, 2008.

Keronen, P., Reissell, A., Rannik, Ü., Pohja, T., Siivola, E., Hiltunen, V., Hari, P., Kulmala, M., and Vesala, T.: Ozone flux measurements over a Scots pine forest using eddy covariance method: performance evaluation and comparison with flux-profile method, Boreal. Environ. Res., 8, 425–443, 2003.

Kolari, P., Pumpanen, J., Kulmala, L., Ilvesniemi, H., Nikinmaa, E., Grönholm, T., and Hari, P.: Forest floor vegetation plays an important role in photosynthetic production of boreal forests, Forest Ecology and Management, 221, 241–248, 2006.

Kolari, P., Lappalainen, H. K., Hänninen, H., and Hari, P.: Relationship between temperature and the seasonal course of photosynthesis in Scots pine at northern timberline and in southern boreal zone, Tellus B, 59, 542–552, doi:10.1111/j.1600-0889.2007.00262.x, http://dx.doi.org/10.1111/j.1600-0889.2007.00262.x, 2007.

Korhonen, H., Lehtinen, K. E. J., and Kulmala, M.: Multicomponent aerosol dynamics model UHMA: model development and validation, Atmospheric Chemistry and Physics, 4, 757–771, doi:10.5194/acp-4-757-2004, http://www.atmos-chem-phys.net/4/757/2004/, 2004.

Kulmala, L., Launiainen, S., Pumpanen, J., Lankreijer, H., Lindroth, A., Hari, P., and Vesala, T.: H2O and CO2 fluxes at the floor of a boreal pine forest, Tellus B, 60, 167–178, doi:10.1111/j.1600-0889.2007.00327.x, http://dx.doi.org/10.1111/j.1600-0889.2007.00327.x, 2008.

Kurpius, M. R. and Goldstein, A. H.: Gas-phase chemistry dominates O3 loss to a forest, implying a source of aerosols and hydroxyl radicals to the atmosphere, Geophysical Research Letters, 30, n/a–n/a, doi:10.1029/2002GL016785, http://dx.doi.org/10.1029/2002GL016785, 1371, 2003.

Kurtén, T., Zhou, L., Makkonen, R., Merikanto, J., Räisänen, P., Boy, M., Richards, N., Rap, A., Smolander, S., Sogachev, A., Guenther, A., Mann, G. W., Carslaw, K., and Kulmala, M.: Large methane releases lead to strong aerosol forcing and reduced cloudiness, Atmospheric Chemistry and Physics, 11, 6961–6969, doi:10.5194/acp-11-6961-2011, http://www.atmos-chem-phys.net/11/6961/2011/, 2011.

Lamaud, E., Carrara, A., Brunet, Y., Lopez, A., and Druilhet, A.: Ozone fluxes above and within a pine forest canopy in dry and wet conditions, Atmospheric Environment, 36, 77–88, 2002.

Lammel, G.: Formation of nitrous acid: parameterisation and comparison with observations, Tech. Rep. REPORT No. 286, Max-Planck-Institut für Meteorologie, 1999.

Launiainen, S., Katul, G. G., Grönholm, T., and Vesala, T.: Partitioning ozone fluxes between canopy and forest floor by measurements and a multi-layer model, Agricultural and Forest Meteorology, 173, 85–99, 2013.

Mammarella, I., Peltola, O., Nordbo, A., Järvi, L., and Rannik, Ü..: Quantifying the uncertainty of eddy covariance fluxes due to the use of different software packages and combinations of processing steps in two contrasting ecosystems, Atmospheric Measurement Techniques, 9, 4915–4933, doi:doi:10.5194/amt-9-4915-2016, 2016.

Massman, W. J.: Toward an ozone standard to protect vegetation based on effective dose: a review of deposition resistances and a possible metric, Atmospheric Environment, 38, 2323–2337, 2004.

Meyers, T. P.: The sensitivity of modeled SO_2 fluxes and profiles to stomatal and boundary layer resistances, Water, Air, and Soil Pollution, 35, 261–278, doi:10.1007/BF00290935, http://dx.doi.org/10.1007/BF00290935, 1987.

Mogensen, D., Smolander, S., Sogachev, A., Zhou, L., Sinha, V., Guenther, A., Williams, J., Nieminen, T., Kajos, M. K., Rinne, J., Kulmala, M., and Boy, M.: Modelling atmospheric OH-reactivity in a boreal forest ecosystem, Atmos. Chem. Phys., 11, 9709–9719, 2011.

Mogensen, D., Gierens, R., Crowley, J. N., Keronen, P., Smolander, S., Sogachev, A., Nölscher, A. C., Zhou, L., Kulmala, M., Tang, M. J., Williams, J., and Boy, M.: Simulations of atmospheric OH, O_3 and NO_3 reactivities within and above the boreal forest, Atmos. Chem. Phys., 15, 3909–3932, 2015.

Nemitz, E., Sutton, M. A., Schjoerring, J. K., Husted, S., and Paul, W. G.: Resistance modelling of ammonia exchange over oilseed rape, Agricultural and Forest Meteorology, 105, 405–425, 2000.

Rannik, Ü., Kolari, P., Vesala, T., and Hari, P.: Uncertainties in measurement and modelling of net ecosystem exchange of a forest, Agricultural and Forest Meteorology, 138, 244–257, 2006.

Rannik, U., Mammarella, I., Keronen, P., and Vesala, T.: Vertical advection and nocturnal deposition of ozone over a boreal pine forest, Atmospheric Chemistry and Physics, 9, 2089–2095, doi:10.5194/acp-9-2089-2009, http://www.atmos-chem-phys.net/9/2089/2009/, 2009.

Rannik, U., Altimir, N., Mammarella, I., Bäck, J., Rinne, J., Ruuskanen, T. M., Hari, P., Vesala, T., and Kulmala, M.: Ozone deposition into a boreal forest over a decade of observations: evaluating deposition partitioning and driving variables, Atmospheric Chemistry and Physics, 12, 12 165–12 182, doi:10.5194/acp-12-12165-2012, http://www.atmos-chem-phys.net/12/12165/2012/, 2012.

Rinne, J., Bäck, J., and Hakola, H.: Biogenic volatile organic compound emissions from the Eurasian taiga: current knowledge and future directions, Boreal Environment Research, 14, 807–826, 2009.

Ruckstuhl, K. E., Johnson, E. A., and Miyanishi, K.: Introduction. The boreal forest and global change, Philosophical Transactions of the Royal Society of London B: Biological Sciences, 363, 2243–2247, doi:10.1098/rstb.2007.2196, http://rstb.royalsocietypublishing.org/content/363/1501/2243, 2008.

Seok, B., Helmig, D., Ganzeveld, L., Williams, M. W., and Vogel, C. S.: Dynamics of nitrogen oxides and ozone above and within a mixed hardwood forest in northern Michigan, Atmospheric Chemistry and Physics, 13, 7301–7320, doi:10.5194/acp-13-7301-2013, http://www.atmos-chem-phys.net/13/7301/2013/, 2013.

Smolander, S., He, Q., Mogensen, D., Zhou, L., Bäck, J., Ruuskanen, T., Noe, S., Guenther, A., Aaltonen, H., Kulmala, M., and Boy, M.: Comparing three vegetation monoterpene emission models to measured gas concentrations with a model of meteorology, air chemistry and chemical transport, Biogeosciences, 11, 5425–5443, 2014.

Sogachev, A.: A note on two-equation closure modelling of canopy flow, Boundary-Layer Meteorol., 130, 423–435, 2009.

Sogachev, A., Menzhulin, G., Heimannn, M., and Lloyd, J.: A simple three dimensional canopy – planetary boundary layer simulation model for scalar concentrations and fluxes., Tellus, 54B, 784–819, 2002.

Stocker, T. F., Qin, D., Plattner, G.-K., Tignor, M., Allen, S. K., Boschung, J., Nauels, A., Xia, Y., Bex, V., and Midgley, P. M.: IPCC, 2013: Climate Change 2013: The Physical Science Basis. Contribution of Working Group I to the Fifth Assessment Report of the Intergovernmental Panel on Climate Change, Cambridge University Press, Cambridge, United Kingdom and New York, NY, USA, 2013.

Wesely, M. L.: Parameterization of surface resistances to gaseous dry deposition in regional-scale numerical models, Atmos. Env., 23, 1293–1304, 1989.

Williams, J., Crowley, J., Fischer, H., Harder, H., Martinez, M., Petäjä, T., Rinne, J., Bäck, J., Boy, M., Dal Maso, M., Hakala, J., Kajos, M., Keronen, P., Rantala, P., Aalto, J., Aaltonen, H., Paatero, J., Vesala, T., Hakola, H., Levula, J., Pohja, T., Herrmann, F., Auld, J., Mesarchaki, E., Song, W., Yassaa, N., Nölscher, A., Johnson, A. M., Custer, T., Sinha, V., Thieser, J., Pouvesle, N., Taraborrelli, D., Tang, M. J., Bozem, H., Hosaynali-Beygi, Z., Axinte, R., Oswald, R., Novelli, A., Kubistin, D., Hens, K., Javed, U., Trawny, K., Breitenberger, C., Hidalgo, P. J., Ebben, C. J., Geiger, F. M., Corrigan, A. L., Russell, L. M., Ouwersloot, H. G., Vilà-Guerau de Arellano, J., Ganzeveld, L., Vogel, A., Beck, M., Bayerle, A., Kampf, C. J., Bertelmann, M., Köllner, F., Hoffmann, T., Valverde, J., González, D., Riekkola, M.-L., Kulmala, M., and Lelieveld, J.: The summertime Boreal forest field measurement intensive (HUMPPA-COPEC-2010): an overview of meteorological and chemical influences, Atmospheric Chemistry and Physics, 11, 10 599–10 618, doi:10.5194/acp-11-10599-2011, http://www.atmos-chem-phys.net/11/10599/2011/, 2011.

Wolfe, G. M. and Thornton, J. A.: The Chemistry of Atmosphere-Forest Exchange (CAFE) Model - Part 1: Model description and characterization, Atmospheric Chemistry and Physics, 11, 77–101, doi:10.5194/acp-11-77-2011, http://www.atmos-chem-phys.net/11/77/2011/, 2011.

Wolfe, G. M., Thornton, J. A., McKay, M., and Goldstein, A. H.: Forest-atmosphere exchange of ozone: sensitivity to very reactive biogenic VOC emissions and implications for in-canopy photochemistry, Atmospheric Chemistry and Physics, 11, 7875–7891, doi:10.5194/acp-11-7875-2011, http://www.atmos-chem-phys.net/11/7875/2011/, 2011.

Wu, Y., Brashers, B., Finkelstein, P. L., and E., P. J.: A multilayer biochemical dry deposition model 1. Model formulation, Journal of Geophysical Research: Atmospheres, 108, doi:10.1029/2002JD002306, http://dx.doi.org/10.1029/2002JD002306, 2003.

Zhou, L., Nieminen, T., Mogensen, D., Smolander, S., Rusanen, A., Kulmala, M., and Boy, M.: SOSAA – a new model to simulate the concentrations of organic vapours, sulphuric acid and aerosols inside the ABL – Part 2: Aerosol dynamics and one case study at a boreal forest site, Boreal Environment Research, 19 (suppl. B), 237–256, 2014.

Zhou, L., Gierens, R., Sogachev, A., Mogensen, D., Ortega, J., Smith, J. N., Harley, P. C., Prenni, A. J., Levin, E. J. T., Turnipseed, A., Rusanen, A., Smolander, S., Guenther, A. B., Kulmala, M., Karl, T., and Boy, M.: Contribution from biogenic organic compounds to particle growth during the 2010 BEACHON-ROCS campaign in a Colorado temperate needleleaf forest, Atmospheric Chemistry and Physics, 15, 8643–8656, doi:10.5194/acp-15-8643-2015, http://www.atmos-chem-phys.net/15/8643/2015/, 2015.